J. Electrochem. Sci. Eng. **14(5)** (2024) 653-669; http://dx.doi.org/10.5599/jese.2383

Open Access : : ISSN 1847-9286
www.jESE-online.org

Original scientific paper

Exploring and evaluating the relationship between *Saccharomyces cerevisiae* biofilm maturation on carbon felt anodes and microbial fuel cell performance

Marcelinus Christwardana[1,2,3,✉], Sri Widodo Agung Suedy[2,3,4], Udi Harmoko[2,5] and Kirana Siffa Sekar Buanawangsa[1]

[1]*Department of Chemistry, Faculty of Science and Mathematics, Diponegoro University. Jl. Prof. Sudarto, SH., Tembalang, Semarang 50275, Indonesia*
[2]*Master Program of Energy, School of Postgraduate Studies, Diponegoro University. Jl. Imam Bardjo, SH., Pleburan, Semarang 50241, Indonesia*
[3]*Research Collaboration Center of Electrochemistry, BRIN – Diponegoro University, Semarang 50275, Indonesia*
[4]*Department of Biology, Faculty of Science and Mathematics, Diponegoro University. Jl. Prof. Sudarto, SH., Tembalang, Semarang 50275, Indonesia*
[5]*Department of Physics, Faculty of Science and Mathematics, Diponegoro University. Jl. Prof. Sudarto, SH., Tembalang, Semarang 50275, Indonesia*

Corresponding authors: ✉ marcelinus@lecturer.undip.ac.id

Received: June 1, 2024; Accepted: August 28, 2024; Published: September 19, 2024

Abstract

Microbial fuel cells (MFCs) hold great promise as sustainable bioenergy sources, with their performance intricately linked to the formation and characteristics of biofilms. This study delves into the bio-electrochemical perspective of biofilms in MFCs, aiming to elucidate their pivotal role in MFC functionality. The investigation focused on a yeast-based MFC operated through 48 h per cycle, with cycle 5 marking the maturation stage of biofilm formation. During this phase, voltage stability was observed, with a stationary phase voltage of 38.9±2.6 mV. Notably, cycle 5 exhibited a significant boost in power density, reaching 8.82 mW m^{-2}, accompanied by the lowest internal resistance of 100 Ω. Furthermore, the electron transfer rate constant from cycle 5 is 1.14±0.02 s^{-1}, 57 times higher than the initial, underscoring biofilm's catalytic potential. Additionally, cyclic voltammetry unveiled non-linear relationships between redox reaction peak current and scan rate, with a consistent ΔE_p of ~219 mV at 100 mV s^{-1}. Importantly, elemental analysis disclosed incorporating diverse elements (Na, Al, Si, P, S, Cl, K, Ca, Cr, and Fe) into the carbon felt, signifying their association with biofilm development. These findings offer critical insights into optimizing MFC performance through biofilm modulation, advancing sustainable bioenergy technologies.

Keywords
Bio-electrochemical fuel cell; carbon anode; biofilm formation; voltage enhancement; biofilm detachment; power density

Introduction

In the pursuit of renewable energy, microbial fuel cells (MFCs) have surfaced as a promising technology that harnesses the power of microorganisms. The formation of biofilms, comprised of complex microbial communities with intricate biochemical interactions, is a significant factor affecting the performance of MFCs. Exploring the biochemical perspective of biofilms in MFCs has the potential to reveal key insights that can improve bioelectricity production. Microbial fuel cells (MFCs) are novel devices that utilize the metabolic processes of microorganisms to directly convert organic matter into electrical energy [1]. MFCs represent a sustainable energy technology that holds great promise for addressing global energy demand and environmental degradation. MFCs rely on the transfer of electrons from the oxidation of organic substrates by microorganisms to an electrode, resulting in the production of electrical current [2]. This novel approach offers numerous benefits, including the utilization of abundant and renewable organic materials, such as effluent, organic waste, and biomass, for electricity production.

In order to optimize and maximize the performance of MFCs, it is necessary to comprehend the numerous factors that affect their operation. MFC efficacy is influenced by various factors, including electrode composition, microorganism type, substrate composition, system configuration, and reactor size [3,4]. Moreover, the formation and characteristics of biofilms in MFCs significantly affect their performance [5]. Understanding the factors that impact MFCs is essential for enhancing their power output, stability, and overall energy conversion efficiency. Remarkably, by delineating the relationships between operational parameters, microbial activities, and electrochemical processes, researchers can develop strategies to improve MFC performance and overcome obstacles such as low power density, electrode contamination, and substrate limitations. Investigating the biochemical perspective of biofilms in MFCs is especially valuable because it allows for a greater understanding of the interplay between microbial metabolism, electron transfer mechanisms, and structure-function relationships of biofilms [6]. Such insights can optimize MFC designs and operating conditions, thereby paving the way for the development of more efficient and sustainable bioelectricity production systems.

Biofilms are multicellular communities of microorganisms that adhere to surfaces and are embedded in a matrix of extracellular polymeric substances (EPS) [7]. They represent a fundamental mode of microbial life that can be found in a wide variety of natural and artificial environments. Biofilms have distinguishing characteristics that set them apart from planktonic microorganisms. Their three-dimensional architecture provides protection and stability to the microbial community they enclose [8]. The EPS matrix acts as an adhesive, facilitating cell-cell and cell-surface interactions while resisting physical and chemical stress [9]. Biofilms are pervasive in nature and can be found in various habitats, including rivers, lakes, oceans, sediment, and even human bodies. They colonize different surfaces, including pebbles, pipelines, medical devices, and submerged structures. Biofilms can grow on surfaces in engineered systems such as water distribution networks, wastewater treatment facilities, and industrial settings.

The prevalence of biofilms is attributable to their ability to adhere to surfaces and establish cooperative interactions between microbial species, resulting in increased survival and growth. Biofilm production can have adverse effects despite the fact that biofilms serve vital roles in natural

ecosystems by contributing to the nutrient cycle [10]. In industrial contexts, biofilms can cause infrastructure deterioration, decreased process efficiency, and heightened contamination risks. In the context of MFCs, biofilms exert a substantial effect on the efficacy of these energy conversion devices. Their composition, structure, and electrochemical interactions affect electron transfer processes and overall MFC performance [11]. Thus, understanding the nature and behavior of biofilms is crucial for a variety of disciplines, including environmental science, healthcare, and biotechnology. Examining the prevalence, composition, and functions of biofilms offers valuable insight into their ecological and industrial implications. Specifically, understanding biofilm dynamics and their effect on bioelectricity production is essential for optimizing the design and operation of MFCs and furthering sustainable energy production in the context of MFCs.

The formation and influence of biofilms on the efficacy of MFCs lend biofilms great significance in the context of MFCs. Microorganisms naturally form biofilms on the electrode surfaces of MFCs, producing a favorable environment for the formation of diverse microbial communities [12]. This biofilm formation is vital to the electron transfer mechanisms that take place within the MFCs system. In a number of ways, the efficacy of MFCs is impacted by the presence of biofilms. First, biofilms offer a larger surface area for microbial attachment, resulting in an increase in microbial population and activity [13]. This results in increased electron transfer rates and superior MFCs performance overall. Additionally, biofilms serve as a protective barrier, shielding the electrode surfaces from physical and chemical disruptions, thereby enhancing the stability and longevity of the MFC systems.

The structure and function of biofilms in MFCs are significant determinants of their performance. Biofilms have an intricate structure composed of microbial cells and the EPS matrix they produce. This structure enables coordinated metabolic and electron transfer processes by facilitating intercellular communication. The EPS matrix functions as a conductive network, enabling efficient electron transfer from microorganisms to the electrode [14]. In addition, the EPS matrix provides mechanical stability to the biofilm, preventing detachment and sustaining a stable microbial community in the MFC system. Understanding the complex structure and function of biofilms in MFCs is indispensable for optimizing MFCs' performance and bioelectricity production. By investigating the dynamics, composition, and interactions of biofilms, researchers can discover strategies to improve electron transfer efficiency, prevent biofilm detachment, and increase system stability. The significance of biofilms in MFCs lies in their ability to influence the microbial community and facilitate efficient electron transfer, paving the way for more efficient and sustainable bioelectricity production.

Yeast *Saccharomyces cerevisiae* offers several advantages as a biocatalyst in microbial fuel cells (MFCs) [15]. Firstly, yeast cells are well-characterized and easy to cultivate, which makes them a practical choice for consistent and reproducible bio-electrochemical studies. Their robust metabolic pathways allow them to efficiently oxidize a wide range of substrates, facilitating electron transfer processes necessary for MFC operation. Additionally, yeast can thrive in various environmental conditions, including anaerobic settings, which are typical for MFC environments. This adaptability enhances their resilience and longevity as biocatalysts. Moreover, yeast produces fewer toxic by-products compared to some bacteria, reducing the risk of electrode fouling and prolonging the operational life of the MFC.

Observing the electrochemical performance of yeast in MFCs provides valuable insights into the status of the biofilm, which is crucial for optimizing MFC efficiency. The biofilm's health and activity directly influence electron transfer rates and overall energy output. By monitoring parameters such

as current density and voltage, the biofilm's metabolic activity and structural integrity can be inferred. Variations in electrochemical performance can indicate changes in biofilm density, viability, and substrate utilization efficiency, enabling timely interventions to maintain optimal MFC function. Thus, electrochemical monitoring serves as a non-invasive and real-time diagnostic tool to assess and enhance biofilm performance in yeast-based MFCs. Focusing on *Saccharomyces cerevisiae* also leverages its established use in various industrial applications, providing a wealth of practical knowledge and technical expertise. This facilitates the translation of laboratory findings into real-world applications, enhancing the scalability and commercial viability of MFC technologies. Overall, the unique combination of scientific understanding, ease of use, and industrial relevance makes *Saccharomyces cerevisiae* an ideal model organism for advancing biofilm research in MFCs.

The objective of this study is to investigate the bio-electrochemical perspective of biofilms in MFCs and to determine their function in MFC performance. This study is significant because it provides insight into the biological mechanisms underlying bioelectricity production in MFCs. Understanding the biochemical perspective of biofilms is essential for optimizing MFC performance, increasing electron transfer efficiency, and devising strategies to boost bioelectricity generation. This study offers an unprecedented investigation into the intriguing and previously uncharted nexus between *Saccharomyces cerevisiae* biofilm maturation on carbon felt anodes and microbial fuel cell performance, promising to unveil unexplored facets of bio-electrochemical systems and beckoning the interest of both seasoned and emerging researchers in this field. This research contributes to the fields of bioelectrochemistry and sustainable energy by expanding our understanding of biofilm dynamics and their effect on MFCs as a renewable energy technology.

Experimental

Microbial fuel cell reactor set-up

A single-chamber cubic reactor made of polyacrylic material (Phychemi Co. Ltd., Beijing, China) was utilized in this study. The selection of polyacrylic material and the specific membrane treatment aimed to enhance the reactor's performance and promote efficient mass transport during the experiment. The geometric surface area of the electrodes was 7 cm^2 and the total volume of the reactor was 30 mL, respectively. Carbon felts (CF) were employed as the anode and cathode. CF based on polyacrylonitrile (PAN) purchased from KWK Steel Co., Ltd (Zhejiang, China) with a diameter of 3 cm was trimmed and inserted into the chamber. Treated Nafion 117 as a membrane separator was used to separate the anode and cathode chambers. The electrodes were then placed in their respective compartments, and the process was carried out at a temperature of about 25 °C, with a conductive stainless-steel wire acting as the current collector. Yeast *Saccharomyces cerevisiae* (Lessafre, Marcq-en-Baroeul, France) were grown in Yeast Peptone D-glucose (YPD). Fresh YPD media comprised of 5 mg mL^{-1} yeast extract (Merck, Darmstadt, Germany), 14 mg mL^{-1} D-glucose (Merck, Darmstadt, Germany), and 2.5 mg mL^{-1} of peptone (Himedia, Mumbai, India) serving as essential nutrients for yeast growth was combined with the 14 mg mL^{-1} yeast *Saccharomyces cerevisiae* serving as biocatalyst [16]. Then, the mixture was diluted with a phosphate buffer saline solution (PBS, 0.1 M, pH 7.4) as an electrolyte. This electrolyte aimed to keep the pH level steady and prevent any detrimental effects of low pH on *Saccharomyces cerevisiae* during the incubation process. Subsequently, the liquid was transferred into the anode chamber of MFCs. In the anode chamber, a tiny magnetic stirrer was placed to ensure the homogeneity of the solution. Following that, the electrodes were placed in the appropriate compartment and the experiment was conducted at a room temperature of approximately 25 °C.

Electrochemical analysis

In half-cell assays, the properties of biofilm grown on anode surfaces were determined. The Arduino-based potentiostat is connected to a computer that is used to conduct electrochemical measurements. The stainless-steel rod was used as the counter electrode, while the Ag/AgCl (soaked in 3.0 M KCl) was used as the reference electrode. As a working electrode, the carbon felt electrode was used. Under atmospheric conditions, the YPD medium, including yeast biocatalyst, was used as the electrolyte. Cyclic voltammetry (CV) experiments were performed at scan rates between 100 and 1600 mV s^{-1} within a potential scan window of -1 to 1 V *vs.* Ag/AgCl, before and after the incubation process of 48 h.

For the single-cell performance analysis test, MFC (microbial fuel cell) yeast was run in seven cycles, each lasting 48 hours (2 days). The purpose of these repetitive cycles was to achieve a stable voltage, which served as an indicator of the attainment of the stationary growth phase of the yeast biofilm. The MFC reactor is connected to a UNI-T UT61E multimeter with an external load of 1000 Ω to measure the voltage. Simultaneously, the overall cell performance, including the output voltage, was evaluated every 10 minutes for each cycle and supplied a new medium every 48 hours. Polarization curves were obtained to determine the maximum power density at the end of each cycle, by gradually applying external resistance in a sequential manner from a resistor box (Elenco RS500 Resistance Substitution Box, Illinois, USA) positioned between the anode and cathode of the yeast MFC, ranging from 10 MΩ to 10 Ω, at 30-minute intervals.

Results and discussion

Full cell analysis

Voltage analysis

Figure 1 depicts the voltage profile of the MFC during the inoculation process, where the YPD medium is used as a nutrient and a new medium is injected at each cycle change. The voltage remains extremely low in the first 25 hours, around 0.0006±0.00002 V, indicating that the yeast is still in the initial adaptation phase. With a voltage value of 0.0054±0.0003 V, the adaptation phase continues until the 48th hour. When new nutrients are introduced at the start of the 2nd cycle, the voltage quickly increases to 0.0227±0.0012 V by the 70th hour.

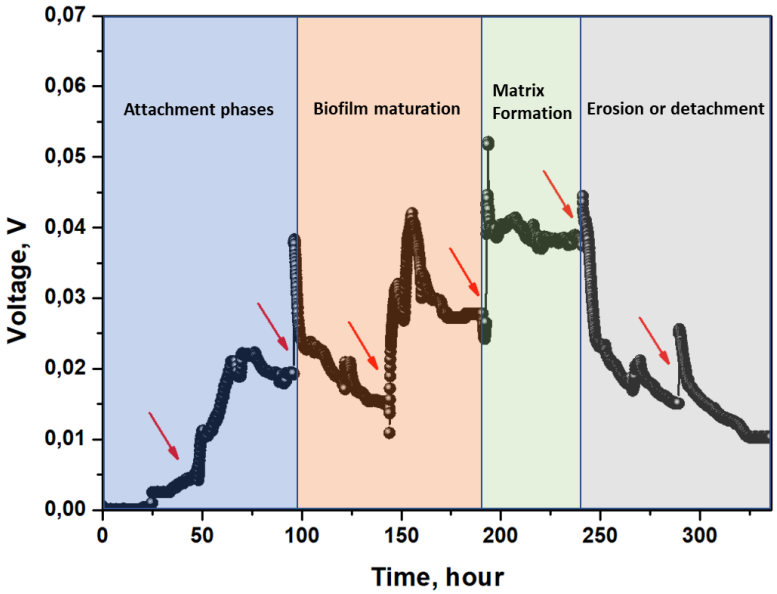

Figure 1. *Voltage measurements during incubation for 7 cycles*

Yeast enters a phase characterized by rapid growth of cells during this time [17]. The voltage then stabilizes and remains constant until the 78th hour, indicating that the yeast has entered the stationary phase, where the growth and mortality rates are balanced. Subsequently, the voltage decreases until the end of the 2nd cycle, reaching 0.0194±0.0021 V, indicating that yeast cells die faster than they are dividing. At the beginning of the 3rd cycle, the MFC voltage increases abruptly to 0.0387±0.0009 V before decreasing progressively to 0.0104±0.0006 V by the end of the third cycle. Both the fourth and fifth cycles display similar patterns. Between 175 and 196 hours of the 4th cycle, the voltage stabilizes at 0.0280±0.0034 V, indicating the stationary phase of the yeast life cycle. The same phenomenon is observed in the 5th cycle, where voltage stability occurs between the 198th and 245th hours, with a stationary phase value of 0.0389±0.0026 V. In contrast to previous cycles, the voltage increases during the 6th cycle is negligible (0.0449±0.0018 V) and is followed by a dramatic decrease until the end of the cycle, when it reaches 0.0153±0.0007 V. The 7th cycle exhibits a rapid initial increase in voltage to 0.0259±0.0011 V, followed by a dramatic decrease to 0.0108±0.0026 V at the cycle's conclusion. The rapid increase in voltage observed at the start of cycles three through five is attributed to the formation of biofilms on the electrodes and the MFC reactor. This expedites the adaptation of newly injected yeast cells, eradicating the need for a lengthy adaptation procedure.

In addition to observing the phenomena that occur in each cycle, it is interesting to discuss the trend that arises from cycle 1 to cycle 7, as it reveals patterns in the phase of biofilm formation. The 1st and 2nd cycles represent the reversible or irreversible attachment phase [18]. Yeast cells have adhesion proteins, such as Flo1p and Flo11p, on their surfaces, which allow them to adhere to solid surfaces by interacting with particular molecules or structures present there [19]. In the 3rd and 4th cycles, the biofilm reaches maturity. Although *Saccharomyces cerevisiae* lacks a well-characterized quorum sensing system, it exhibits population-dependent behaviors [20]. For example, attaining a critical population density within a biofilm can induce changes in gene expression or metabolic activity, thereby fostering biofilm maturation. Within the yeast colonies, matrix formation occurs during the 5th cycle. Once attached, *Saccharomyces cerevisiae* cells produce an extracellular matrix of polysaccharides, proteins, and other molecules. This matrix functions as a scaffold, holding the biofilm's cells together and providing structural stability. Its composition can vary, but it typically consists of polysaccharides such as glucans and mannans, as well as proteins such as Flo1p and Flo11p [21]. The biofilm increases in size and complexity as yeast cells continue to proliferate and produce more extracellular matrix. The matrix not only reinforces the structure of the biofilm but also retains water and nutrients, thereby creating a favorable microenvironment for the yeast cells [22]. Biofilm detachment occurs during the 6th and 7th cycles, causing the yeast biofilm to detach from the electrode surface. Environmental conditions, nutrient availability, physical disturbances, and chemical signals can all induce detachment [23]. The disintegration of the extracellular matrix that holds the biofilm together facilitates detachment. Matrix disruption can be aided by enzymes produced by the biofilm community, such as dispersal enzymes or enzymes involved in matrix degradation. In addition, physical forces or shear stress from fluid flow can diminish the interactions between cells and the surface, thereby increasing the likelihood of detachment [24]. This detachment phase causes a significant voltage decrease during the 6th and 7th cycles. The formation phase of yeast biofilm on the surface of the electrode is proven by the weight of the biofilm attached to the electrode surface.

Power density analysis during biofilm formation

Each cycle of a microbial electrochemical system's power density is represented by the data provided. Various factors, such as biofilm maturation, population density, extracellular matrix formation, and environmental conditions, affect the power density values, as shown in Figure 2. The first cycle's power density is relatively modest at 0.056 mW m^{-2}. This could be attributed to the onset of biofilm formation and electrochemical reactions. During this phase, the microbial community adapts to its surroundings and develops the necessary electron transfer pathways. As the system enters its second cycle, the power density reaches 0.71 mW m^{-2}, a significant increase. This increase suggests increased microbial activity and enhanced electrochemical performance. The biofilm has presumably reached maturity, resulting in enhanced electron transfer between microbial cells and the electrode surface. In cycles three and four, the trend continues with power density values of 2.095 and 2.523 mW m^{-2}, respectively. These increased values suggest further optimization and expansion of the biofilm, resulting in an increase in energy production. The microbial community has probably attained a critical population density, resulting in increased electron transfer and metabolic activity in the biofilm. Cycle five demonstrates a significant increase in power density to 3.877 mW m^{-2}. This may have been caused by a combination of factors. At this juncture, the biofilm has established a robust extracellular matrix, which provides structural stability and enhanced electron transfer pathways [25]. In addition, the increased size and complexity of the biofilm may have improved nutrient and electron transport, resulting in a higher power output. However, the power density decreases slightly in subsequent cycles. The sixth cycle power density is 2.824 mW m^{-2}, and the seventh cycle power density is 0.94 mW m^{-2}. Several factors may have contributed to this decline. It is plausible that detachment of the biofilm or changes in environmental conditions impacted the stability and electron transfer efficacy of the biofilm. Changes in nutrient availability or physical disturbances may have disrupted the structure of the biofilm, resulting in decreased energy production.

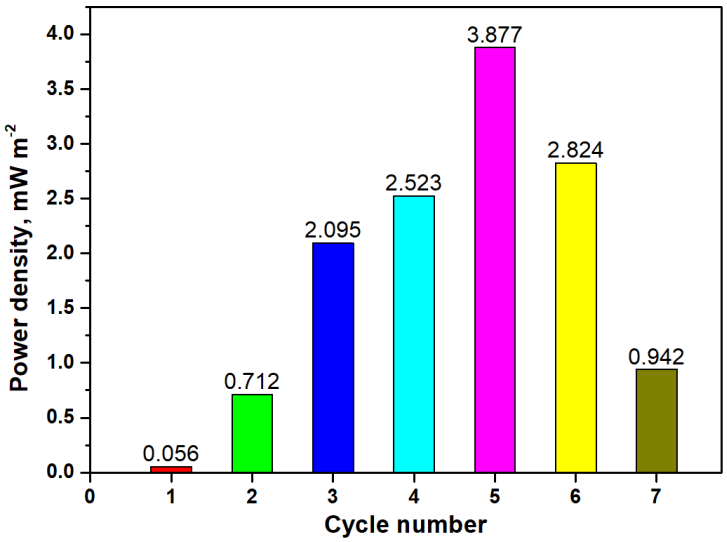

Figure 2. *Power density reached in each cycle of incubation*

Polarization and power curves analysis

Figure 3(a) shows the yeast microbial fuel cell (MFC) polarization curve measured at the end of each cycle. The open circuit voltage (OCV) ranges from 0.38 to 0.43 V across all cycles, which deviates from the optimal value of 1.23 V. Several factors, including inherent electrochemical reactions, kinetics and microbial activity, internal resistance, mass transport limitations, and electrode kinetics and

catalysts, contribute to this discrepancy [26]. In the activation loss region, the voltage drops precipitously owing to the activation overpotential. When electrochemical reactions at the electrode surfaces occur at a relatively sluggish rate, activation overpotential develops. This is due to lethargic reaction kinetics, high activation energy, or insufficient electrode/electrolyte interfaces. Consequently, a greater voltage is required to initiate these reactions, resulting in a discernible voltage drop within the activation loss region of the polarization curve. In addition, the charge transfer resistance at the interface between the electrode and electrolyte contributes to the activation overpotential. This resistance inhibits electron transport between the electrode and electrolyte. A greater charge transfer resistance amplifies the activation overpotential, resulting in a greater voltage decrease within the activation loss region. In the region of ohmic loss, the voltage decreases progressively or appears to level off. The presence of a constant line in the ohmic loss region indicates that the voltage drop across the system is predominantly caused by resistance rather than electrochemical reactions [27]. The ohmic resistance is the resistance encountered by the passage of current through the electrolyte, electrode materials, and other conductive elements in the system. It is directly correlated to the current passing through the circuit and can be affected by variables such as the conductivity of the electrolyte, dimensions of the electrodes, and their properties. The horizontal line indicates that the electrochemical system's efficacy is primarily constrained by its internal resistance. The concentration loss region displays a significant decrease in voltage, which is predominantly a result of concentration overpotential. Concentration overpotential occurs when the transport or availability of substrates or products at the electrode-electrolyte interface are restricted. This may be the result of sluggish diffusion through the electrolyte or mass transport limitations resulting from insufficient mingling or convective flow [28]. As substrates are consumed or products accumulate near the surface of an electrode, concentration gradients form, resulting in concentration overpotential. The decrease in voltage in the concentration loss region indicates the increased mass transport resistance. The electrochemical reaction consumes substrates faster than they can be replenished, diminishing their concentration near the electrode surface. This limited availability of reactants causes a concentration overpotential and a substantial voltage decrease. In addition, the accumulation of reaction products close to the electrode surface may contribute to concentration overpotential and voltage decrease in the concentration loss region [29].

Figure 3(b) illustrates the power density profiles of the microbial fuel cells (MFCs) at each cycle. The utmost value for maximum power density (MPD) is reached in the 5th cycle with a remarkable value of 8.82 mW m^{-2}, as shown in the graph.

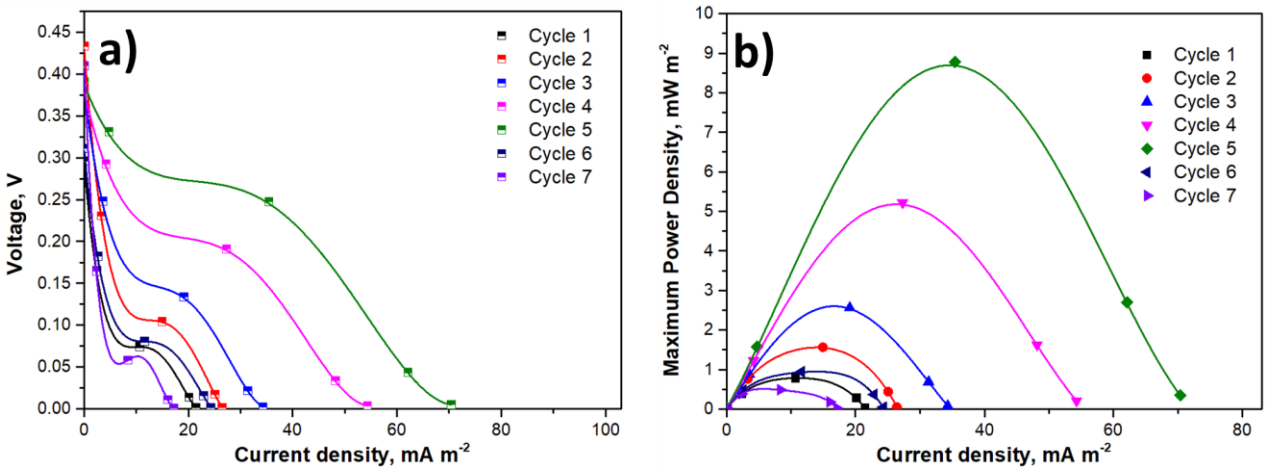

Figure 3. *(a) Polarization and (b) maximum power density curves of MFCs for every cycle of incubation*

This value represents a substantial increase relative to the first cycle and is 18 times higher than the 7th cycle. The trend of power density is similar to power production during the incubation process. Biofilms create a structured environment that facilitates efficient electron transfer within the microbial community and between the cells and the electrode surface. This enhanced electron transfer capability results in increased power generation and an increase in the overall maximal power density. It is important to note that biofilm stability is essential for sustaining power production. Stable biofilms with resilient structural integrity are better able to maintain a continuous electron transfer process, resulting in enhanced power generation and higher maximal power density.

Polarization internal resistance

In MFCs, the relationship between the internal resistance of a fuel cell, as determined by polarization curves, and biofilm formation phenomena is crucial. By measuring the slope of the ohmic loss on the polarization curve, the internal resistance of MFCs can be determined and the results are shown in Figure 4 [30]. The formation and characteristics of biofilm can substantially affect the fuel cell's internal resistance. This internal resistance follows the opposite trend as power density, where the power density decreases as the internal resistance rises, and *vice versa* [31]. The 5th cycle polarization curve has the lowest internal resistance, while the 7th cycle polarization curve has the maximum internal resistance with a value of 143.72 Ω. As the biofilm develops on the electrode surface, the internal resistance of the fuel cell may increase. The biofilm functions as an additional resistance barrier that impedes the movement of ions and electrons, resulting in increased internal resistance values [32]. The thickness of biofilm can also affect the internal resistance. As a result of their conductivity, thicker biofilms can reduce internal resistance. The matrix of yeast biofilms is composed of EPS, which may contain conductive materials such as humic substances or conductive polymers [33]. These components contribute to the biofilm's overall electrical conductivity by forming a network that enables electron transport. During metabolic processes, redox reactions can generate free electrons within the biofilm, contributing to its conductivity. However, excessively dense biofilms impede ion and electron transport, resulting in increased internal resistance. This is because the distance that ions and electrons must travel to reach the electrode surface is increased for a biofilm layer that is too thick.

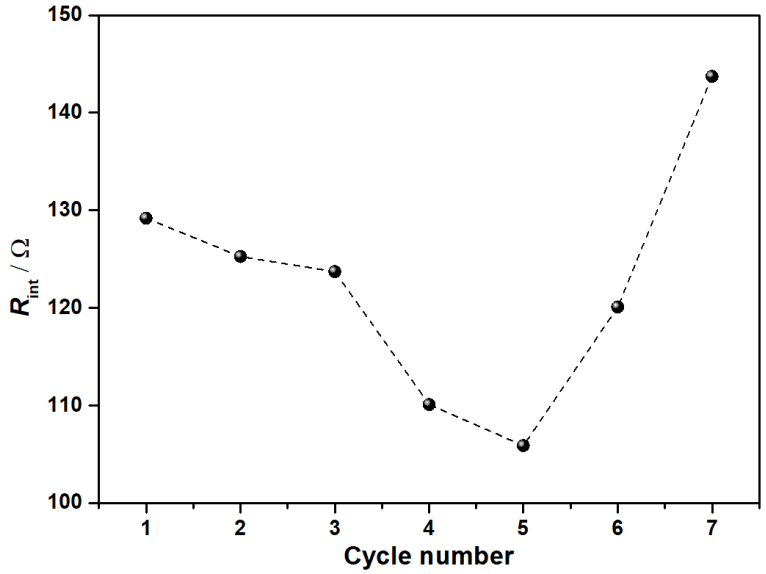

Figure 4. *Internal resistance of MFCs system for every cycle of incubation*

Half-cell analysis

Analysis of cyclic voltammetry results

Performing half-cell analysis in the form of cyclic voltammetry (CV) is of utmost importance in order to validate the performance of a yeast microbial fuel cell (MFC) at different stages of biofilm growth. The CVs of yeast cultures at different stages of the experimental cycle are depicted in Figure **5**. Specifically, illustrates the CVs measured at the beginning of the cycle, the end of cycle 1 (attachment), the end of cycle 5 (maturation), and the end of cycle 7 (detachment). Upon careful observation of the provided visual representation, it becomes evident that a multitude of noteworthy elements are worthy of attention and analysis. In all CV curves, it is observed that an oxidation peak occurs within the potential range of 0.4 to 0.5 V *vs.* Ag/AgCl reference electrode, while a reduction peak is observed within the potential range of 0 to 0.2 V *vs*. Ag/AgCl reference electrode. The peak of the oxidation phenomenon entails the intricate process by which organic substances undergo oxidation *via* the catalytic activity of yeast [34]. This process can occur in a dynamic, unconfined state or within a pre-existing biofilm matrix. The ultimate outcome of this oxidation event is the conversion of organic materials into carbon dioxide (CO_2), protons (H^+), and electrons (e^-). The reduction peak observed in this study corresponds to the O_2 reduction reaction that occurs at the carbon electrode. The utilization of carbon felt as the anode material and the implementation of a semi-anaerobic incubation condition allow for the controlled entry and diffusion of oxygen into the solution. In the subsequent stages, namely the attachment and maturation phases, which correspond to the 1st and 5th cycles, respectively, it can be observed that the electrical double layer in the CV curve undergoes a shift towards higher positive current density values (as depicted in Figure 5(a).

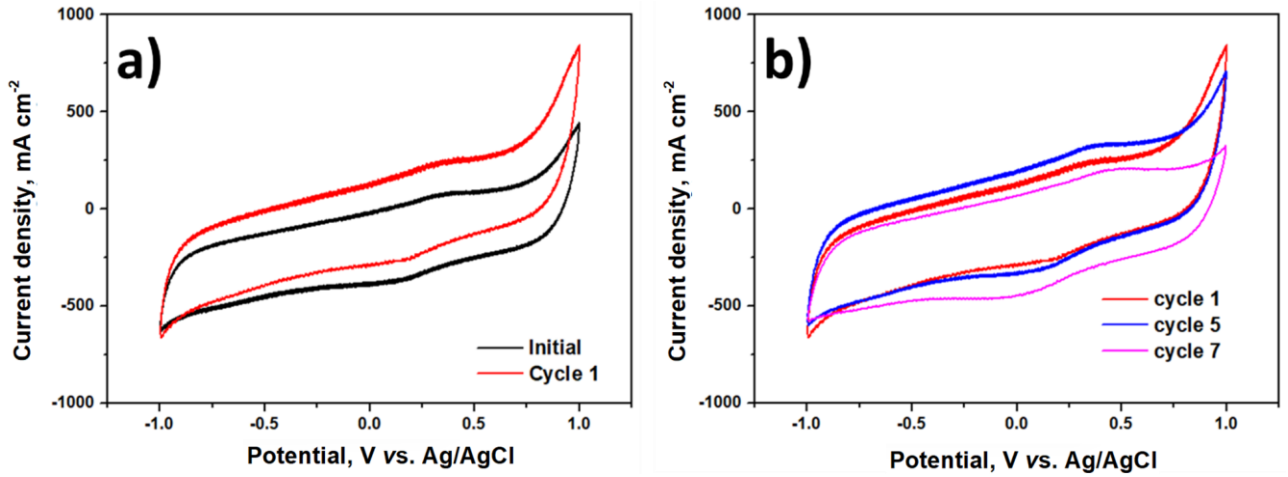

Figure 5*. CV graphs of CF anode at (a) initial and the end of cycle 1, and (b) at the end of cycles 1, 5, and 7*

The aforementioned observation suggests the occurrence of an oxidation mechanism involving organic substances, which serve as a substrate for yeast metabolism. As a result of this process, CO_2 gas, protons, and electrons are generated. The electrons produced by the yeast are subsequently collected by the working electrode. The observed increase in the upward trajectory of the CV curve during the 5th cycle exhibited a greater magnitude in comparison to that of the 1st cycle. The observations indicate that during the 5th cycle, substantial amounts of biofilm have developed on the electrode surface, resulting in an increased capacity for the conversion of organic materials into product metabolism. In the third observation, it is noted that the electrical double layer of the CV during the detachment phase of the 7th cycle has exhibited an increase in comparison to its initial

position. However, this increase is not found to surpass the magnitude of the increases observed during the 1st or 5th cycle, as depicted in Figure 5(b). The findings of this study confirm that during the 7th cycle, a notable occurrence occurred wherein multiple strata of the yeast biofilm adhered to the electrodes were shed, presumably resulting in their demise. Consequently, the population of yeast cells capable of metabolizing organic substances and generating electrons was significantly diminished.

In order to provide further elucidation on the growth of yeast biofilm on each CF electrode, the coverage of electroactive biocatalyst (Γ) encompassing the CF electrode was determined through the utilization of the Randles-Ševčik equation [35], as provided in Eq. (1):

$$\Gamma = \frac{4RTI_p}{\upsilon n^2 F^2 A} \quad (1)$$

where Γ is the surface concentration of the electroactive biocatalyst, I_p is the peak current, R is the universal gas constant, T is temperature, A is the area of the electrode, υ is the scan rate, n is the number of electrons involved in a redox reaction, and F is Faradaic constant. The resulting values obtained from these calculations are presented in Table 1. The obtained values are determined by analyzing the oxidation peaks of the CV graph, obtained from electroactive substances content intracellularly within yeast cells [36]. The values of the parameter Γ at the initial incubation and the end of incubation cycles 1, 5, and 7 are 0.155, 0.387, 0.410, and 0.348 μmol cm^{-2}, respectively. In line with the findings from the voltage analysis conducted in the preceding section, it was observed that the biofilm exhibited a progressive increase in growth until the end of cycle 5. However, during cycle 7, a decline in biofilm growth was observed, primarily attributed to a substantial mortality rate among yeast cells. Consequently, this phenomenon led to a diminished production of electrons.

Table 1. *The biocatalyst surface coverage on the surface of CF electrode*

Condition	Biocatalyst surface coverage, μmol cm^{-2}*
initial	0.155
end of cycle 1	0.387
end of cycle 5	0.410
end of cycle 7	0.348

*based on oxidation reaction of electroactive substances inside the yeast cell

Rate determining step and electron transfer rate constant

In order to examine the rate-determining step (RDS) and determine the electron transfer rate constant (ETRC), the CV of the CF anode was assessed after both the first cycle and the fifth cycle, using various scan rates ranging from 100 to 1600 mV s^{-1}. The observation of a rise in reduction and oxidation peaks with increasing scan rate is seen in Figure 6(a) and Figure 6(d). As the scanning rate is increased, the redox processes occurring inside the electrodes have a reduced duration for attaining equilibrium. Consequently, it is possible for redox processes to not achieve complete equilibrium, leading to the manifestation of more pronounced or distinct oxidation and reduction peaks. The augmentation of the scan rate may lead to a concomitant rise in polarization loss occurring at the electrodes. This implies that the electrode potential may not attain its anticipated value when the scanning rates are increased. The observed augmentation in oxidation and reduction peaks may be attributed to an amplified polarization loss.

The redox reaction peak current density *vs*. potential scan rate was measured in Figure 6(b) and Figure 6(e) to investigate the route of the rate-determining reaction. It shows that the redox reaction peak current is non-linearly linked to the potential scan rate, while the difference in the

peak potential ΔE_p, is ~219 mV at a scan rate of 100 mV s^{-1}. This demonstrates that all catalysts are controlled by a diffusion, and the redox reactions occur in a quasi-reversible reaction region [37,38]. In order to generate protons and electrons, yeast is required to undergo a preliminary process of food consumption, followed by a subsequent metabolic activity that occurs over an extended duration.

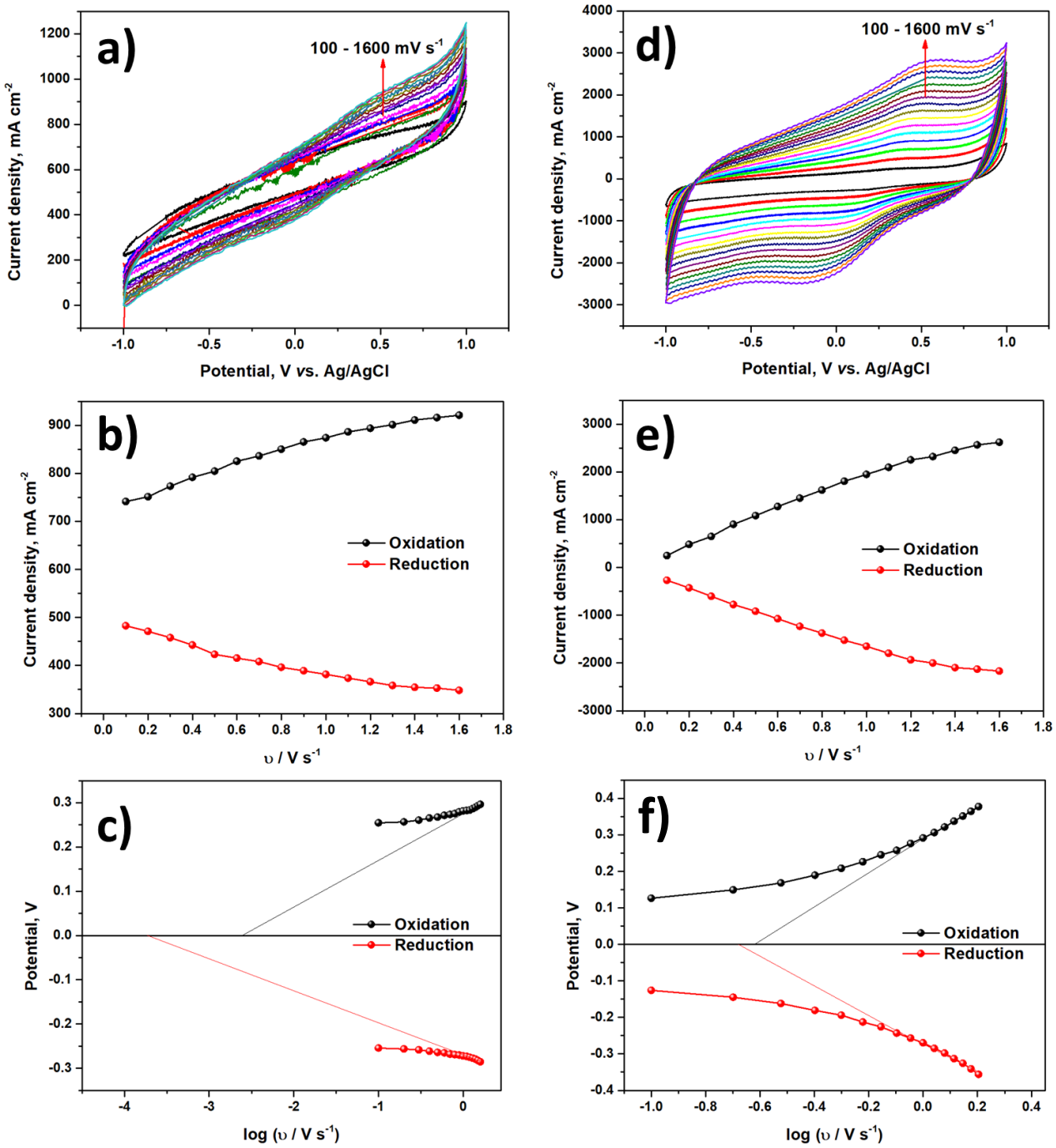

Figure 6*. CV graphs of CF anode at different scan rates (a, d), oxidation and reduction peak current densities vs. scan rate (b, e), and Laviron plots (c, f) at the start of cycle 1 (a,b,c) and end of cycle 5 (d,e,f)*

In order to provide more clarification on the catalytic activity of the respective catalysts, the electron transfer rate constant (k_s) was determined by the use of Laviron's formula (Eq. 2), as seen in Figure 6c and 6f [39].

$$\log k_s = \alpha\log(1-\alpha)+(1-\alpha)\log\alpha-\log(RT/nF\upsilon)-\alpha(1-\alpha)nF\Delta E_p/2.3RT \quad (2)$$

where k_s is electron transfer rate constant, α is charge transfer coefficient, R is universal gas constant, T is temperature, n is the number of electrons involved in a redox reaction, F is Faradaic constant, υ is potential scan rate, and ΔE_p is peak potential difference. Based on the calculations, it was seen that the k_s value of the CF anode at the end of the fifth cycle exhibited a higher value (1.14±0.02 s^{-1}), which is 57 times higher compared to the first cycle, which has a value of 0.02±0.00 s^{-1}. The observed pattern aligns well with the polarization data, suggesting that the electron transfer rate in the fifth cycle experiences a significant rise due to the development of a biofilm composed of yeast.

SEM and EDX analysis

The electrode morphology of the yeast microbial fuel cell (MFC) was assessed through the utilization of scanning electron microscopy (SEM) images, both prior to and subsequent to the completion of five operational cycles. In accordance with the observations made in Figure 7(a), it is evident that the carbon felt fiber does not exhibit any discernible biofilm formation. The observed phenomenon pertains solely to the discernible presence of dirt particles adhering to the surface of the carbon felt material, a consequence of its manufacturing process. In Figure 7(b), yeast colonies are observed on the surface of the carbon felt fiber. The observed phenomenon can be attributed to the adhesion mechanism of yeast cells with carbon felt, as well as the concurrent formation of C-N bonds, electrostatic interactions, and hydrophobic interactions. The observed proliferation of yeast colonies indicates that carbon felt exhibits a favorable level of biocompatibility with yeast. This is substantiated by the notable interactions and cohesive bonds observed among yeast colonies, resulting in the formation of a biofilm on the surface of the electrode material [40].

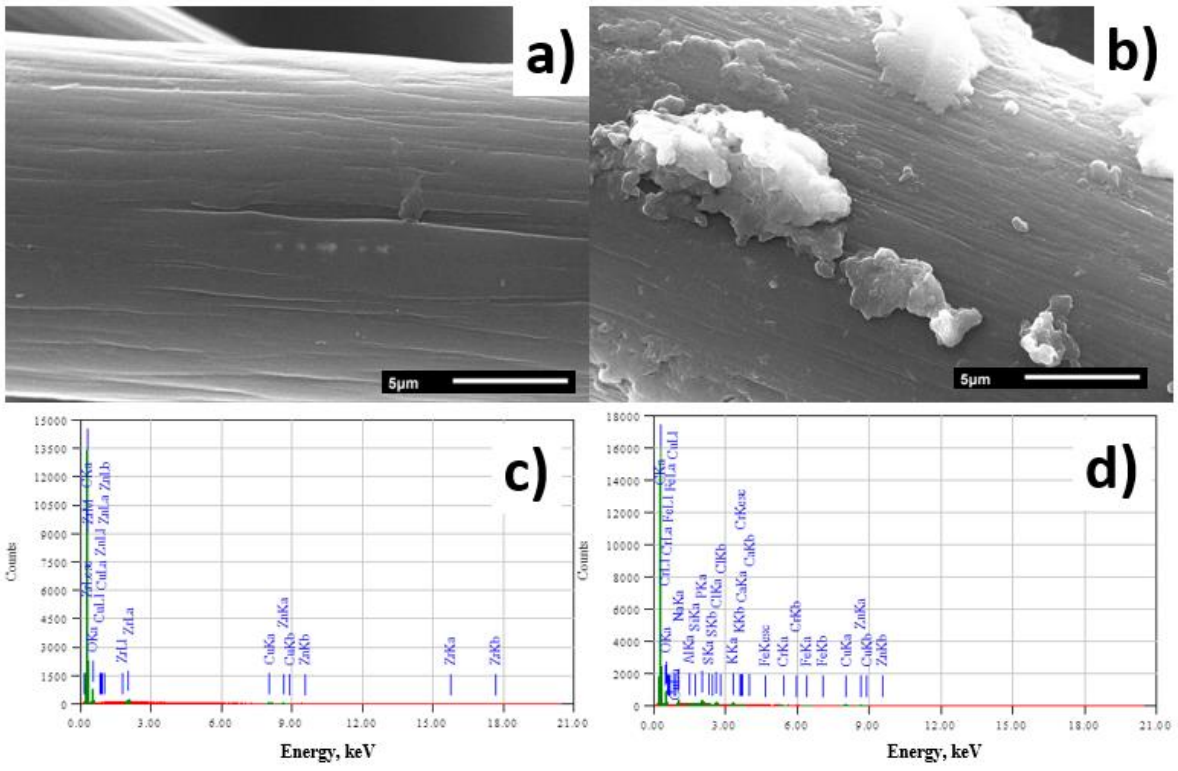

Figure 7. *SEM images (above) and EDX spectra (below) of CF anode at: a) and c) initial, b) and d) end of 5th cycle*

The objective of the EDX analysis is to provide evidence supporting the presence of a biofilm on the surface of the carbon-felt material. This can be inferred by observing an augmentation in the concentrations of specific elements. In accordance with the EDX spectra findings presented in Figure

7(c), it is evident that the prevailing compositions observed in carbon felt primarily consist of C and O. These two elements are widely recognized as the principal constituents of carbon felt, while Cu, Zn, and Zr were impurities with very small composition, less than 0.1 %. The other elements were not detected in large quantities, suggesting the absence of biofilm formation on the surface of the carbon-felt material. In terms of carbon felt, it is worth noting that a biofilm is responsible for its growth, as depicted in Figure 7(d). It is interesting to observe that this growth process introduces various additional elements into the carbon felt, including Na, Al, Si, P, S, Cl, K, Ca, Cr, and Fe. The observed manifestation of these elements is hypothesized to be attributable to the biofilm formation, thereby providing substantiation for the robust growth of the biofilm on the surface of the carbon-felt material [41].

Conclusion

The analysis of a yeast MFC across different biofilm growth stages offers key insights into its electrochemical and biological processes. Voltage analysis during MFC cycles reveals crucial phases of yeast adaptation and biofilm formation. Voltage rises significantly from an initial 0.0006±0.00002 to 0.0389±0.0026 V by the 5th cycle, showing biofilm's impact. Power density analysis reinforces the link between biofilm maturity and enhanced electron transfer, peaking at the 5th cycle with a remarkable 8.82 mW m^{-2}, a stark improvement from the initial 0.056 mW m^{-2}, underscoring biofilm's influence. Polarization and power curves unveil factors affecting internal resistance, with the lowest resistance at the 5th cycle and the highest resistance at the 7th cycle, showcasing the biofilm's role. Half-cell analysis performed through cyclic voltammetry experiments quantifies biofilm growth *via* surface coverage (Γ) values, reaching a peak of 0.410 µmol cm^{-2} at the 5th cycle, which is a significant increase from the initial 0.155 µmol cm^{-1}. Rate-determining step and electron transfer rate constant analysis demonstrate increased k_s value up to 1.14±0.02 s^{-1} during the 5th cycle, emphasizing the biofilm impact on electron transfer kinetics. SEM and EDX surface analyses visually confirmed the presence of a mature biofilm on the carbon felt electrode, validating its biocompatibility with yeast cells and showing an increase in various elements, affirming biofilm growth. These quantitative findings underscore the critical role of biofilm development in enhancing MFC performance, offering valuable insights into microbial electrochemical systems for sustainable energy generation and environmental remediation.

Acknowledgement: *Authors thanks to Biochemistry Laboratory, Department of Chemistry UNDIP for the support of its facilities.*

Funding: *This project was fully supported by DIPA Sekolah Pascasarjana Universitas Diponegoro 2023, with contract number: 266/UN7.M1/PP/III/2023.*

Disclosure of interest: *The authors declare that they have no known competing financial interests or personal relationships that could have appeared to influence the work reported in this paper.*

Data availability: *The datasets generated and analyzed during the current study are available from the corresponding author on reasonable request.*

Author contribution: *All authors contributed to the study conception and design. Material preparation, data collection and analysis were performed by K.S. Sekar and M. Christwardana. The first draft of the manuscript was written by M. Christwardana, U. Harmoko, and S.W.A. Suedy, and all authors commented on previous versions of the manuscript.*

References

[1] T. Naaz, A. Kumar, A. Vempaty, N. Singhal, S. Pandit, P. Gautam, S. P. Jung, Recent advances in biological approaches towards anode biofilm engineering for improvement of extracellular electron transfer in microbial fuel cells, *Environmental Engineering Research* **28(5)** (2023) 220666. https://doi.org/10.4491/eer.2022.666

[2] I. Chattopadhyay, T. M. Usman, S. Varjani, Exploring the role of microbial biofilm for industrial effluents treatment, *Bioengineered* **13(3)** (2022) 6420-6440. https://doi.org/10.1080/21655979.2022.2044250

[3] J. V. Boas, V. B. Oliveira, M. Simões, A. M. Pinto, Review on microbial fuel cells applications, developments and costs, *Journal of Environmental Management* **307** (2022) 114525. https://doi.org/10.1016/j.jenvman.2022.114525

[4] D. A. Jadhav, A. A. Carmona-Martínez, A. D. Chendake, S. Pandit, D. Pant, Modeling and optimization strategies towards performance enhancement of microbial fuel cells, *Bioresource Technology* **320** (2021) 124256. https://doi.org/10.1016/j.biortech.2020.124256

[5] L. Zhou, Y. Wu, S. Zhang, Y. Li, Y. Gao, W. Zhang, L. Tian, T. Li, Q. Du, S. Sun, Recent development in microbial electrochemical technologies: Biofilm formation, regulation, and application in water pollution prevention and control, *Journal of Water Process Engineering* **49** (2022) 103135. https://doi.org/10.1016/j.jwpe.2022.103135

[6] Z. Syed, M. Sogani, J. Rajvanshi, & K. Sonu, Electroactive biofilm and electron transfer in microbial electrochemical systems, *Scaling Up of Microbial Electrochemical Systems* (2022) 29-48. https://doi.org/10.1016/B978-0-323-90765-1.00003-4

[7] M. Pal, A. Shrivastava, R. K. Sharma, Electroactive biofilm development on carbon fiber anode by Pichia fermentans in a wheat straw hydrolysate based microbial fuel cell, *Biomass and Bioenergy* **168** (2023) 106682. https://doi.org/10.1016/j.biombioe.2022.106682

[8] R. Hartmann, P. K. Singh, P. Pearce, R. Mok, B. Song, F. Díaz-Pascual, J. Dunkel, K. Drescher, Emergence of three-dimensional order and structure in growing biofilms, *Nature Physics* **15(3)** (2019) 251-256. https://doi.org/10.1038/s41567-018-0356-9

[9] H. Li, H. Liu, L. Zhang, A. Hieawy, Y. Shen, Evaluation of extracellular polymeric substances matrix volume, surface roughness and bacterial adhesion property of oral biofilm, *Journal of Dental Sciences* **18(4)** (2023) 1723-1730. https://doi.org/10.1016/j.jds.2022.12.022

[10] Y. Dhar, Y. Han, Current developments in biofilm treatments: Wound and implant infections, *Engineered Regeneration* **1** (2020) 64-75. https://doi.org/10.1016/j.engreg.2020.07.003

[11] J. Greenman, I. Gajda, J. You, B. A. Mendis, O. Obata, G. Pasternak, I. Ieropoulos, Microbial fuel cells and their electrified biofilms, *Biofilm* **3** (2021) 100057. https://doi.org/10.1016/j.bioflm.2021.100057

[12] A. A. Mier, H. Olvera-Vargas, M. Mejía-López, A. Longoria, L. Verea, P. J. Sebastian, D. M. Arias, A review of recent advances in electrode materials for emerging bioelectrochemical systems: From biofilm-bearing anodes to specialized cathodes, *Chemosphere* **283** (2021) 131138. https://doi.org/10.1016/j.chemosphere.2021.131138

[13] X. Wu, Z. Chen, Z. Lv, L. Zhang, F. Xin, Y. Li, G. Liu, W. Dong, P. Wei, H. Jia, Enhanced chloramphenicol-degrading biofilm formation in microbial fuel cells through a novel synchronous acclimation strategy, *Journal of Cleaner Production* **317** (2021) 128376. https://doi.org/10.1016/j.jclepro.2021.128376

[14] Y. Hu, Y. Wang, X. Han, Y. Shan, F. Li, L. Shi, Biofilm biology and engineering of Geobacter and Shewanella spp. for energy applications, *Frontiers in Bioengineering and Biotechnology* **9** (2021) 786416. https://doi.org/10.3389/fbioe.2021.786416

[15] M. Verma, V. Mishra, Recent trends in upgrading the performance of yeast as electrode biocatalyst in microbial fuel cells, *Chemosphere* **284** (2021) 131383. https://doi.org/10.1016/j.chemosphere.2021.131383
[16] M. Christwardana, G. E. Timuda, N. Darsono, H. Widodo, K. Kurniawan, D. S. Khaerudini, Fabrication of a polyvinyl alcohol-bentonite composite coated on a carbon felt anode for improving yeast microbial fuel cell performance, *Journal of Power Sources* **555** (2023) 232366. https://doi.org/10.1016/j.jpowsour.2022.232366
[17] M. Christwardana, H. Hadiyanto, S. A. Motto, S. Sudarno, K. Haryani, Performance evaluation of yeast-assisted microalgal microbial fuel cells on bioremediation of cafeteria wastewater for electricity generation and microalgae biomass production, *Biomass and Bioenergy* **139** (2020) 105617. https://doi.org/10.1016/j.biombioe.2020.105617
[18] P. Zhang, C. Yang, Y. Xu, H. Li, W. Shi, X. Xie, M. Lu, L. Huang, W. Huang, Accelerating the startup of microbial fuel cells by facile microbial acclimation, *Bioresource Technology Reports* **8** (2019) 100347. https://doi.org/10.1016/j.biteb.2019.100347
[19] C. Bouyx, M. Schiavone, J. M. François, FLO11, a developmental gene conferring impressive adaptive plasticity to the yeast Saccharomyces cerevisiae, *Pathogens* **10(11)** (2021) 1509. https://doi.org/10.3390/pathogens10111509
[20] M. Xu, M. Sun, X. Meng, W. Zhang, Y. Shen, W. Liu, Engineering Pheromone-Mediated Quorum Sensing with Enhanced Response Output Increases Fucosyllactose Production in Saccharomyces cerevisiae, *ACS Synthetic Biology* **12(1)** (2022) 238-248. https://doi.org/10.1021/acssynbio.2c00507
[21] Y. Zhao, J. Wang, Q. Fu, H. Zhang, J. Liang, W. Xue, G. Zhao, H. Oda, Characterization and Antioxidant Activity of Mannans from Saccharomyces cerevisiae with Different Molecular Weight, *Molecules* **27(14)** (2022) 4439. https://doi.org/10.3390/molecules27144439
[22] K. Quan, J. Hou, Z. Zhang, Y. Ren, B. W. Peterson, H. C. Flemming, C. Mayer, H. J. Busscher, H. C. van der Mei, Water in bacterial biofilms: pores and channels, storage and transport functions, *Critical reviews in microbiology* **48(3)** (2022) 283-302. https://doi.org/10.1080/1040841X.2021.1962802
[23] P. K. Jha, H. Dallagi, E. Richard, M. Deleplace, T. Benezech, C. Faille, Does the vertical vs horizontal positioning of surfaces affect either biofilm formation on different materials or their resistance to detachment? *Food Control* **133** (2022) 108646. https://doi.org/10.1016/j.foodcont.2021.108646
[24] T. Wang, Z. Guo, Y. Shen, Z. Cui, A. Goodwin, Accumulation mechanism of biofilm under different water shear forces along the networked pipelines in a drip irrigation system, *Scientific Reports* **10(1)** (2020) 6960. https://doi.org/10.1038/s41598-020-63898-5
[25] S.M. Tan, S.A. Ong, L.N. Ho, Y.S. Wong, C.Z.A. Abidin, W.E. Thung, T.P. Teoh, Polypropylene biofilm carrier and fabricated stainless steel mesh supporting activated carbon: Integrated configuration for performances enhancement of microbial fuel cell, *Sustainable Energy Technologies and Assessments* **46** (2021) 101268. https://doi.org/10.1016/j.seta.2021.101268
[26] A. Erensoy, S. Mulayim, A. Orhan, N. Cek, A. Tuna, N. Ak, The system design of the peat-based microbial fuel cell as a new renewable energy source: The potential and limitations, *Alexandria Engineering Journal* **61(11)** (2022) 8743-8750. https://doi.org/10.1016/j.aej.2022.02.020
[27] G. Geetanjali, S. Rawat, R. Rani, S. Kumar, Kinetic modeling for miniaturize single-chambered microbial fuel cell: effects of biochemical reaction on its performance. *Environmental Science and Pollution Research* **31** (2023) 39015–39024. https://doi.org/10.1007/s11356-023-28798-x

[28] J. Yang, Y. B. Sim, H. H. Joo, J. H. Jung, S. H. Kim, Enhanced continuous biohydrogen production using dynamic membrane with conductive biofilm supporter, *Bioresource Technology* **377** (2023) 128900. https://doi.org/10.1016/j.biortech.2023.128900
[29] P. Y. Zhang, Z. L. Liu, Experimental study of the microbial fuel cell internal resistance, *Journal of Power Sources* **195(24)** (2010) 8013-8018. https://doi.org/10.1016/j.jpowsour.2010.06.062
[30] B. E. Logan, *Microbial fuel cells*, John Wiley & Sons, City, Country, 2008, doi or ISBN or URL
[31] X. Zhao, Y. Zhou, J. Xu, G. Chen, Y. Fang, T. Tat, X. Xiao, Y. Song, S. Li, J. Chen, Soft fibers with magnetoelasticity for wearable electronics, *Nature Communications* **12(1)** (2021) 6755. https://doi.org/10.1038/s41467-021-27066-1
[32] R. G. Remya, B. R. Sreelekshmy, B. I. Bijimol, A. Ratheesh, S. M. A. Shibli, Strategic regulation of barrier characteristics of biofilms to enhance the extracellular electrogenic performance in MFCs: an electrochemical dynamic evaluation study, *Sustainable Energy & Fuels* **7(13)** (2023) 3122-3133. https://doi.org/10.1039/D3SE00464C
[33] W. Yang, J. Li, Q. Fu, L. Zhang, Z. Wei, Q. Liao, X. Zhu, Minimizing mass transfer losses in microbial fuel cells: Theories, progresses and prospectives, *Renewable and Sustainable Energy Reviews* **136** (2021) 110460. https://doi.org/10.1016/j.rser.2020.110460
[34] J. V. Boas, L. Peixoto, V. B. Oliveira, M. Simões, A. M. F. R. Pinto, Cyclic voltammetry study of a yeast-based microbial fuel cell, *Bioresource Technology Reports* **17** (2022) 100974. https://doi.org/10.1016/j.biteb.2022.100974
[35] L. Fotouhi, M. Fatollahzadeh, M. M. Heravi, Electrochemical behavior and voltammetric determination of sulfaguanidine at a glassy carbon electrode modified with a multi-walled carbon nanotube, *International Journal of Electrochemical Science* **7(5)** (2012) 3919-3928. https://doi.org/10.2116/analsci.28.497
[36] Y. Hubenova, M. Mitov, Extracellular electron transfer in yeast-based biofuel cells: A review, *Bioelectrochemistry* **106** (2015) 177-185. https://doi.org/10.1016/j.bioelechem.2015.04.001
[37] M. Christwardana, Y. Kwon, Yeast and carbon nanotube based biocatalyst developed by synergetic effects of covalent bonding and hydrophobic interaction for performance enhancement of membraneless microbial fuel cell, *Bioresource Technology* **225** (2017) 175-182. https://doi.org/10.1016/j.biortech.2016.11.051
[38] M. Christwardana, D. Frattini, K. D. Duarte, G. Accardo, Y. Kwon, Carbon felt molecular modification and biofilm augmentation via quorum sensing approach in yeast-based microbial fuel cells, *Applied Energy* **238** (2019) 239-248. https://doi.org/10.1016/j.apenergy.2019.01.078
[39] E. J. J. Laviron, General expression of the linear potential sweep voltammogram in the case of diffusionless electrochemical systems, *Journal of Electroanalytical Chemistry and Interfacial Electrochemistry* **101(1)** (1979) 19-28. https://doi.org/10.1016/S0022-0728(79)80075-3
[40] L. A. Estudillo-Wong, C. Guerrero-Barajas, J. Vázquez-Arenas, N. Alonso-Vante, Revisiting Current Trends in Electrode Assembly and Characterization Methodologies for Biofilm Applications, *Surfaces* **6(1)** (2023) 2-28. https://doi.org/10.3390/surfaces6010002
[41] M. Christwardana, J. Joelianingsih, L. A. Yoshi, Performance of yeast microbial fuel cell integrated with sugarcane bagasse fermentation for cod reduction and electricity generation, *Bulletin of Chemical Reaction Engineering & Catalysis* **16(3)** (2021) 446-458. https://doi.org/10.9767/bcrec.16.3.9739.446-458